Characterization of Levitated Superfluid Helium Drops in High Vacuum

C. D. Brown,[1,2,3] Y. Wang,[4] M. Namazi,[4,5] G. I. Harris,[4,5] M. T. Uysal,[4] and J. G. E. Harris[1,4,5]

[1]*Department of Physics, Yale University, New Haven, CT 06520*
[2]*Department of Physics, University of California, Berkeley CA 94720*
[3]*Challenge Institute for Quantum Computation, University of California, Berkeley CA 94720*
[4]*Department of Applied Physics, Yale University, New Haven, CT 06520*
[5]*ARC Centre of Excellence for Engineered Quantum Systems,*
School of Mathematics and Physics, The University of Queensland, Brisbane, QLD, Australia and
[6]*Yale Quantum Institute, Yale University, New Haven, CT 06520*
(Dated: September 14, 2021)

We describe measurements of the thermal, mechanical, and optical properties of drops of superfluid [4]He that are magnetically levitated in high vacuum. The drops have radius ~ 200 µm, cool by evaporation to temperatures ~ 300 mK, and can be trapped indefinitely in a background vapor pressure $\sim 10^{-8}$ mBar. Measurements of the drops' evaporation rate, normal modes of motion, and optical whispering gallery modes are found to agree with well-established models.

Superfluid helium drops offer a combination of isolation, low temperature, superfluidity, and experimental access that is unique among condensed matter systems. These features make it possible to address a number of questions in chemistry and physics [1, 2]. Such drops have been used to cool a range of molecular species to ~ 400 mK, facilitating precision spectroscopy and studies of cold chemical reactions [3–6]. In addition, the drops themselves are interesting for studies of classical and quantum fluid dynamics [7–11], and may be well-suited for studies of macroscopic quantum phenomena [12].

In practice, the scientific questions that can be addressed by an isolated helium drop depend on its size, temperature, and lifetime, and on the experimental probes that can be applied to it. For example, a drop must exceed a certain size to become superfluid, or to serve as a host for chemical dopants. The drop's size sets the frequency and energy scales of its internal excitations (such as its vorticity and the acoustic modes of its bulk and surface). Its size also determines its ability to host optical whispering gallery modes (WGMs). Low temperature is required for the drop to become superfluid, and to isolate quantum coherent effects in the drop's excitations. Lastly, some experimental probes require the drop to be trapped; in these cases, its lifetime will be limited by its evaporation rate, which depends strongly on temperature.

A number of approaches have been used to trap superfluid drops. Electric trapping has confined mm-scale drops, but requires the drops to be charged [13]. Neutral drops may be optically trapped, but to date practical laser-power considerations have limited this approach to µm-scale drops [14]. Magnetic trapping has been used to confine cm-scale, electrically-neutral drops [15]. In principle, each of these approaches is compatible with operation in high vacuum; however, studies to date of trapped superfluid drops have been carried out in the presence of He vapor whose density is high enough that the drop's temperature is set by the temperature of its enclosure.

An important alternative to trapping drops is to study them in free fall[16–22]. Freely falling droplets can be produced with radii ranging from nm to µm, typically via expansion through a nozzle into a high vacuum chamber. These droplets fall for ~ 10 ms before they are destroyed, either by measurement or by colliding with the end of the vacuum chamber. In this time, the droplet's temperature is found to be accurately described by a model of free evaporation into perfect vacuum [23], with [4]He droplets reaching temperatures as low as $T_{\mathrm{drop}} \sim 380$ mK.

In this paper we describe studies of mm-scale, electrically-neutral, superfluid [4]He drops that are trapped by diamagnetic levitation in high vacuum. We have measured their thermal, mechanical, and optical properties, including their evaporation rate, heat load, and temperature; their capillary modes and center-of-mass motion; and their medium-finesse optical WGMs. These measurements show good agreement with theoretical predictions, and demonstrate that superfluid drops can be trapped indefinitely with $T_{\mathrm{drop}} \sim 330$ mK.

A schematic illustration of the experiment is shown in Fig. 1a. Levitation is provided by a non-uniform superconducting solenoid housed in the [4]He bath space of a cryostat. As described elsewhere, levitation occurs when $B_z \partial_z B_z = \mu_0 \rho g / |\chi|$, with this levitation point being stable when $\partial_{ii} B^2 > 0$ for all $i \in \{x, y, z\}$ [15]. Here, z is the axial coordinate, B_z is the axial magnetic field component, μ_0 is the permeability of free space, $\rho = 145$ kg/m^3 is the density of liquid [4]He, g is the gravitational acceleration and $\chi = -1.89 \times 10^{-6}$ is the volume diamagnetic susceptibility of [4]He.

The solenoid is designed so that stable levitation is achieved for 115 A $< I <$ 118 A, where I is the current in the solenoid. Varying I within this range translates the levitation point vertically, and can be used to vary the drop shape (i.e., from prolate to oblate) [24].

Drops are produced and trapped in a custom-built cell that fits in the cryostat's vacuum space and extends into the magnet's bore. The temperature of the cell walls is
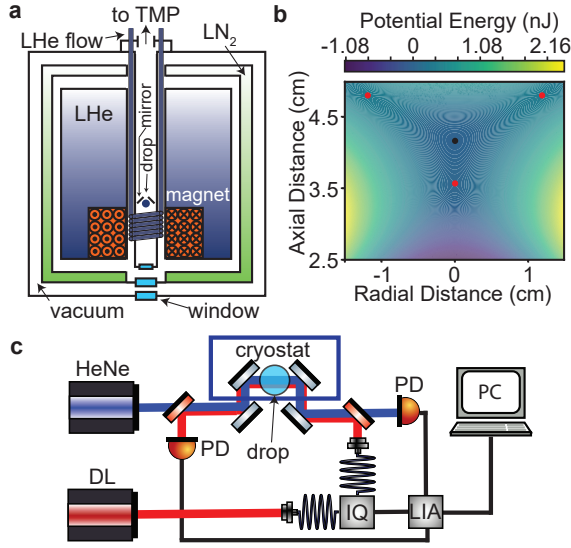
FIG. 1. Experimental schematic. (a) Cross-sectional view of the cryostat and the experimental cell. (b) The potential energy of a drop (with $R = 1$ mm), showing a stable equilibrium point (black circle) and saddle points (red circles). The axes are the axial and radial distance from the solenoid's center. (c) The measurement apparatus, showing the two lasers, optical modulator (IQ), photodiodes (PD), and lock-in amplifier (LIA)

FIG. 2. A levitated drop. Inset: an image of a levitated ^{4}He drop with $R \approx 1.5$ mm shortly after it is generated. The drop radius (circles) as a function of time after the end of the rapid evaporation period. The red curve is a fit to the sum of an exponential and a linear function (the linear portion is the dashed line). The statistical uncertainty in R is ~ 10 nm. The blue band shows the systematic uncertainty.

controlled by a liquid ^{4}He flow line. Optical access to the trapping region is provided by windows in the cryostat and cell.

To produce a levitated drop, I is fixed and the cell is cooled by the ^{4}He flow line. The cell is then filled with a controlled quantity of ^{4}He, which produces a puddle at the bottom of the cell. Next, the cell is opened to a turbomolecular pump (TMP), which causes the puddle to boil aggressively. In the subsequent seconds, a fog of μm-scale droplets aggregates in the levitation region and then coalesces into a single mm-scale drop at the levitation point. The inset of Fig. 2 shows a levitated drop with $R = 1.0$ mm roughly 1 s after opening the cell to the TMP.

After the drop has been trapped, the TMP continues to evacuate the cell and the liquid remaining in the puddle cools to $T_{\text{cell}} \sim 1.5$ K, corresponding to vapor in the cell at pressure $P_{\text{cell}} \sim 1$ mbar. This vapor damps the drop's initial motion and maintains thermal contact between the drop and the cell walls. Fixing the drop's temperature while also pumping on it causes the drop to gradually shrink. After roughly five minutes the puddle is completely depleted, causing P_{cell} to decrease sufficiently that thermal contact between the drop and the cell walls is broken. The drop's thermal isolation is evidenced by the fact that R appears constant (within the resolution of the imaging system) for several hours.

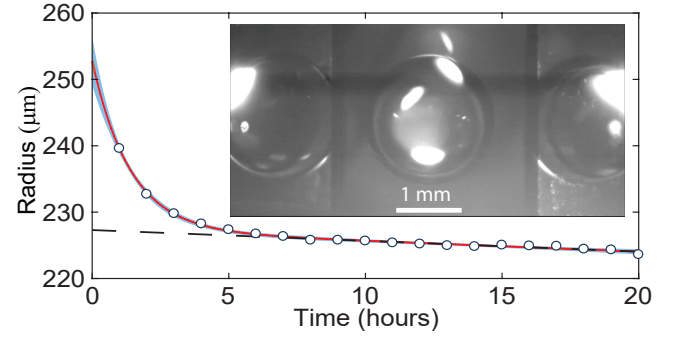Closer examination of these images shows that the drop does continue to evaporate, but at a greatly reduced rate. To measure small changes in R, we use standard image processing techniques [25] to determine the drop's edge in each video frame. This shape is fit to a circle whose radius is a fit parameter. The value of R returned by this fit is averaged over 1,200 images (acquired in 60 s) to produce each of the data points shown in Fig. 2. From this data, the evaporation rate can be seen to decrease in the first few hours after trapping, and then to become roughly constant. A linear fit to the last 12 hours of data gives an average evaporation rate $\dot{R} = (0.44 \pm 0.04)$ Å/s. According to the model described in Ref.[23], this corresponds to $T_{\text{drop}} \approx 330$ mK and a heat load $\dot{Q} \sim 30$ pW on the drop. As described below, the likely source of this heat is residual He vapor in the cell.

The drop's center-of-mass (COM) motion is measured using the setup shown in Fig. 1c. A diode laser (DL) with wavelength $\lambda = 1,064$ nm passes though the drop so that it is refracted by an angle that depends on the drop's position. This deflection is measured using a photodiode. (The other laser shown in Fig. 1b is not used for these measurements; its use is described below).

Fig. 3a shows the COM motion for various values of the magnet current I. No deliberate drive was applied to the drop; the observed motion is the drop's steady-state response to mechanical vibrations in the cryostat. For each value of I, the data show peaks corresponding to the three normal modes of motion in the trap. The resonant frequencies f_{COM} of these modes are shown as a function of I in Fig. 3b. The dashed lines are the frequencies calculated (without free parameters) for a cylindrically-symmetric trapping field whose symmetry axis is colinear with gravity. In this model, the radial and axial frequencies are $\omega_r = (-\chi/(\mu_0\rho)(1/2(\partial_z B_z)^2 - B_z\partial_{zz}B_z))^{1/2}$ and $\omega_z = (-2\chi/(\mu_0\rho)((\partial_z B_z)^2 + B_z\partial_z B_z))^{1/2}$ respectively, with the magnetic field and its derivatives evaluated at the levitation point [25] (the numerical values of these
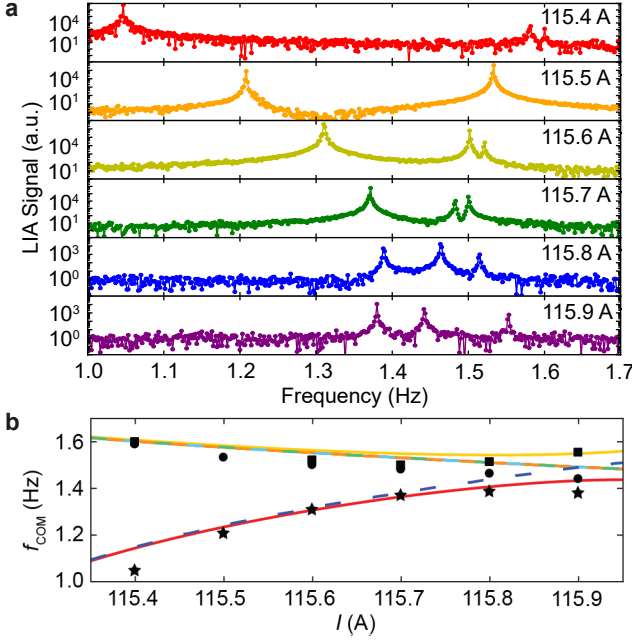
FIG. 3. Center-of-mass (COM) motion of a levitated drop. (a) The power spectral density of the COM motion for various magnet currents. (b) The frequencies of the normal modes versus the magnet current. Black markers: frequencies determined by fitting the data in (a). Dashed lines: the calculated radial (light blue and light green) and axial (dark blue) frequencies assuming the magnets axis is parallel to gravity. Solid lines (red, orange, yellow): the best fit of the data for a magnetic trap that is tilted with respect to gravity.

FIG. 4. Optical WGMs. (a) The lock-in signal produced by optical transmission through a superfluid drop with $R = 240 \pm 1$ μm. (b) The integral of the data in (a). (c) The calculated finesse for WGMs with $q \in \{1, 2, 3\}$. (d) The calculated splitting between TE and TM modes, $\Delta\tau/\delta t$, with $q \in \{1, 2, 3\}$.

quantities are known from the magnet design).

While this model reproduces the qualitative features in the f_{COM}, it does not capture their behavior near the predicted degeneracy at $I = 115.9$ A. The solid lines in Fig. 3b show a fit to a model that incorporates a relative angle θ between gravity and the trap's symmetry axis [25]. Using θ as a fitting parameter returns $\theta = (0.27 \pm 0.11)°$. We note that this misalignment may result from a tilt of the cryostat, or from a deformation of the trapping fields due to magnetic materials near the cell.

The drops levitated here are nearly spherical, with index of refraction $n_{\text{He}} = 1.028$ for visible and near-infrared wavelengths, and vanishingly small absorption (predicted to be $\sim 10^{-9}$ m^{-1} for $T_{\text{drop}} = 330$ mK [14, 26]). As a result they are expected to host optical WGMs whose finesse increases rapidly with R for $R > 0.1$ mm [12].

To characterize these WGMs, we use the setup shown in Fig. 1b. Here the DL is focused at the center of the drop and its intensity is modulated at a fixed frequency close to the resonance of the drop's $\ell_{\text{cap}} = 2$ capillary mode (described below). The optical dipole force exerted by the DL beam excites this capillary mode, which effectively modulates R (more precisely, the drop's circumference in the plane of the WGM is modulated). At the
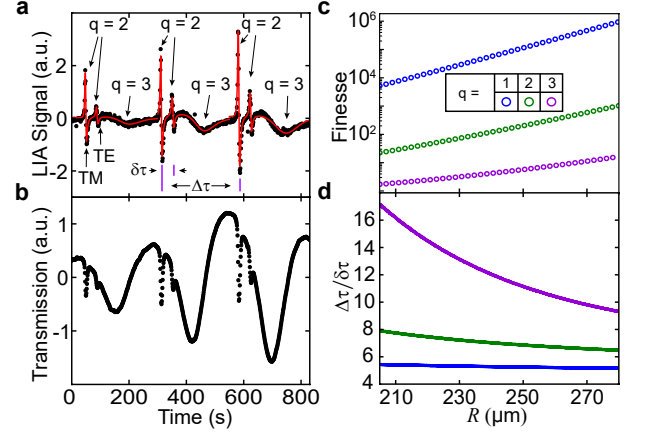
same time, an intensity-stabilized HeNe laser ($\lambda = 633$ nm) is focused at the drop's edge, and its transmission is recorded using a lock-in amplifier (LIA). In addition to the modulation produced by the drop's capillary mode, the drop's evaporation causes R to slowly decrease with time; as a result the LIA signal is approximately proportional to the derivative of the drop's transmission with respect to R.

Fig. 4a shows a typical record from the LIA for a drop trapped with $I = 116$ A. Analysis of video images taken during these measurements gives $R = 240 \pm 1$ μm. Fig. 4b shows the same data integrated with respect to time, giving a signal proportional to the optical transmission through the drop. The data show a pattern of features that repeats with a period ~ 300 s. Each feature corresponds to a WGM that is tuned through resonance with the HeNe by the drop's evaporation. Each repetition of the pattern corresponds to the drop's circumference changing by $\lambda_{\text{HeNe}}/n_{\text{He}}$ (equivalent to the WGM's angular index $\ell \approx 2,380$ changing by 1), which tunes the cavity through one free spectral range (FSR).

Within each of the three FSRs shown in Fig. 4a, the data is fit to the sum of three (once-differentiated) Lorentzians, with each Lorentzian's center position, linewidth, and amplitude used as fit parameters. The result is the red curve in Fig. 4a. These fits give the finesse $\mathcal{F} = 36 \pm 2$ for the largest feature, $\mathcal{F} = 30 \pm 3$ for the middle feature, and $\mathcal{F} = 1.9 \pm 0.1$ for the broadest feature. These value are the averages over the three FSRs shown in Fig. 4a.

To determine the identities of these modes, Fig. 4c shows the calculated $\mathcal{F}$ for WGMs in a sphere with index of refraction 1.028, as a function of the sphere's radius [27]. Results are shown for both TE and TM po-

larizations, and for values of the WGM's radial index $1 \geq q \geq 3$ (where $q - 1$ gives the number of a radial electric field nodes within the drop). Fig. 4d shows the calculated splitting between TE and TM modes (with all other mode indices equal). These plots indicate that the broadest feature in each FSR corresponds to $q = 3$ modes (their linewidth is too large to resolve the TE and TM modes separately), and that the two narrower features correspond to TE and TM modes with $q = 2$.

The measured linewidths of these $q = 2$ modes are roughly three times greater than in the calculation shown in Fig. 4c. This is consistent with the small ellipticity ($\epsilon \sim 10^{-5}$) expected for this value of R and I [24]. Ellipticity splits the $(2\ell + 1)$-fold degeneracy over the WGM's azimuthal index m into resonances which are shifted from the spherical (i.e., $\epsilon = 0$) resonance by [28]

$$\Delta\omega_\epsilon \equiv |\omega_{q,\ell,m} - \omega_{q,\ell,m+1}| \approx ck_{q,\ell,m}\epsilon\frac{(|m| + 1/2)}{\ell^2}. \quad (1)$$

The splittings within this multiplet (i.e. between modes with m differing by ± 1) are all much smaller than the expected WGM linewidth, so they result in an unresolved band whose width (i.e., for $0 \leq m \leq 2,380$ in Eq. 1) would result in an apparent finesse $\mathcal{F}_\epsilon = 46$ for the $q = 2$ modes.

The fit in Fig. 4 a also gives the ratio between the FSR and the splitting between the TE and TM $q = 2$ modes as 6.6 ± 0.1. This is in good agreement with the calculated value of 6.9 (Fig. 4d).

We did not observe the $q = 1$ WGMs, whose finesse is expected to be $\sim 10^4$. This is likely because of the poorer mode-matching between these modes and the HeNe beam, and because the drop's evaporation tuned these modes through resonance too quickly to be recorded with our data sampling rate (1 Hz).

Since the passage of each FSR corresponds to the drop circumference changing by $\lambda_{\mathrm{HeNe}}/n_{\mathrm{He}}$, we can use the duration $\Delta\tau$ of each FSR as a measurement of the drop's evaporation rate $\dot{R} = \lambda_{\mathrm{HeNe}}/2\pi n_{\mathrm{He}}\Delta\tau$. The evaporation model given in Refs. [12, 23] can then be used to infer T_{drop} and $\dot{Q}$ from $\dot{R}$.

This approach is illustrated in Fig. 5, which shows data for a drop with $R = 207.5 \pm 1$ μm (as determined by image analysis). The optical transmission through this drop (not shown) has features similar to those in Fig. 4a, which are fit to determine $\Delta\tau$. Figs. 5a,b show T_{drop} and $\dot{Q}$ inferred in this manner as a function of P_{DL}, the power of the DL incident on the drop. The data are consistent with a heat load proportional to P_{DL}, along with a background heat load ~ 35 pW. While the former contribution could reflect absorptive heating of the drop by the DL, the coefficient of proportionality (3×10^{-9}) is roughly three orders of magnitude greater than expected [14, 26]. If, instead, the observed heatload is attributed to He gas in the cell (assumed to be at the
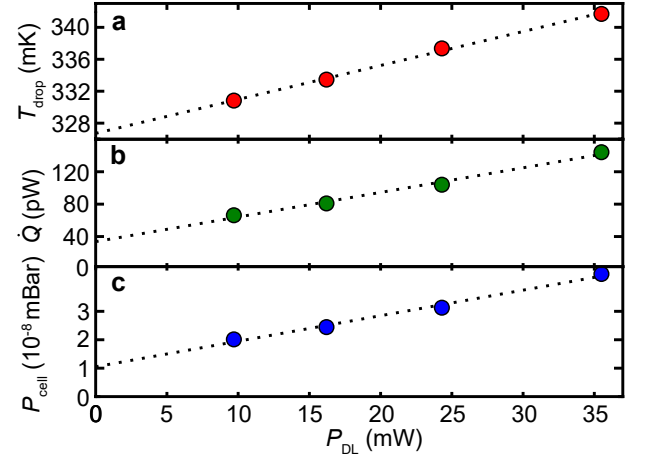

FIG. 5. The drop's thermal properties. (a) The drop temperature. (b) The heat load on the drop. (c) The background pressure in the cell. These quantities are obtained from measurements of $\dot{R}$, and are plotted as a function of the power of the laser incident on the drop. The dashed lines are linear fits.

temperature of the cell walls), the corresponding pressure P_{cell} is shown in Fig. 5c. We attribute the increase in P_{cell} with increasing P_{DL} to the absorption of laser light by various objects in the cell.

Vibrations of the drop for which the restoring force is dominated by surface tension are known as capillary modes. These modes' oscillation frequencies are given by

$$f_{\ell_{\mathrm{cap}}} = \frac{1}{2\pi}\sqrt{\frac{\ell_{\mathrm{cap}}(\ell_{\mathrm{cap}} + 1)(\ell_{\mathrm{cap}} - 2)\sigma}{\rho R^3}}, \quad (2)$$

where $\ell_{\mathrm{cap}} \in \{2, 3, 4, ...\}$ and $\sigma = 3.75 \times 10^{-4}$ J/m^2 is the surface tension of superfluid liquid ^{4}He [29]. To drive these modes, the DL is focused at the drop's center and its intensity is modulated at frequency f_{drive}. The modes' response is monitored by recording the transmission of the HeNe beam through the drop. This beam's position is chosen to avoid the optical WGMs, so its transmission is modulated because the capillary modes deflect the beam.

Fig. 6 shows the frequencies and linewidths of the first several resonances measured in a drop with $R = 246 \pm 0.7$ μm and $T_{\mathrm{drop}} \approx 330$ mK. The frequencies and linewidths are determined by fitting each resonance (as shown in the inset). Assuming that each resonance corresponds to a distinct value of ℓ_{cap} (except for $\ell_{\mathrm{cap}} = 9$, which did not produce a measurable signal) the resonance frequencies are found to agree with Eq. 2 to better than 1%.

These modes' linewidths $\Gamma_{\ell_{\mathrm{cap}}}$ are shown in Fig. 6b, along with the values expected from the damping of capillary modes by inelastic scattering of thermal phonons from the drop's surface: [30]
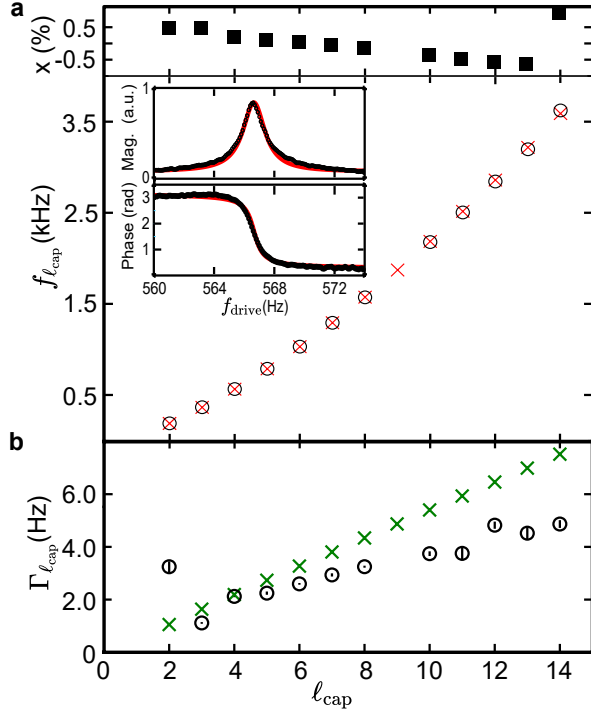
FIG. 6. Capillary mode resonances. (a) The measured (circles) and expected (crosses) resonance frequencies. Inset: the complex response of the $\ell_{\mathrm{vib}} = 4$ mode (black), along with the best fit (red). Upper panel: the residual X between the measured and predicted frequencies. (b) The measured (circles) and expected (crosses) damping rates.

$$\frac{\Gamma_{\ell_{\mathrm{cap}}}}{2\pi} = \frac{\pi^2 \hbar \mathcal{K}}{60 \rho_0} \left(\frac{k_B T}{\hbar u_c}\right)^4, \qquad (3)$$

where $\mathcal{K} = (\ell_{\mathrm{cap}}(\ell_{\mathrm{cap}} - 1)(\ell_{\mathrm{cap}} + 2))^{1/3}/R$ and $u_c = 238$ m/s is the speed of sound in liquid ^{4}He. While this prediction shows qualitative agreement with the data, we note two discrepancies. The first is in the average slope of $\Gamma_{\ell_{\mathrm{cap}}}$ vs. ℓ_{cap}. This slope is predicted to be $\propto T_{\mathrm{drop}}^{-4}$, and would agree with the observed slope if one were to take $T_{\mathrm{drop}} = 310$ mK. However this would correspond to an evaporation rate $\sim 4\times$ smaller than observed. The second discrepancy is in the damping rates for $\ell_{\mathrm{cap}} = 2$ and $\ell_{\mathrm{cap}} = 3$, which depart from the simple trend predicted by Eq. 3.

Both discrepancies may have their origin in the fact that Eq. 3 is derived under the assumption that phonons which are inelastically scattered by the surface fully thermalize before being scattered again. However the mean free path of phonons in superfluid helium $\Lambda \propto T^{-4}$, with $\Lambda = 4.5$ mm for $T = 330$ mK [31]. Furthermore the phonon thermalization time $\Lambda/u_c \approx 16$ μs $\ll f_{\ell_{\mathrm{cap}}}^{-1}$ for $2 \leq \ell_{\mathrm{cap}} \leq 14$. Thus, a thermal phonon in the drops studied here will scatter many times from an effectively stationary drop surface. The damping of capillary modes in this regime has not been calculated.
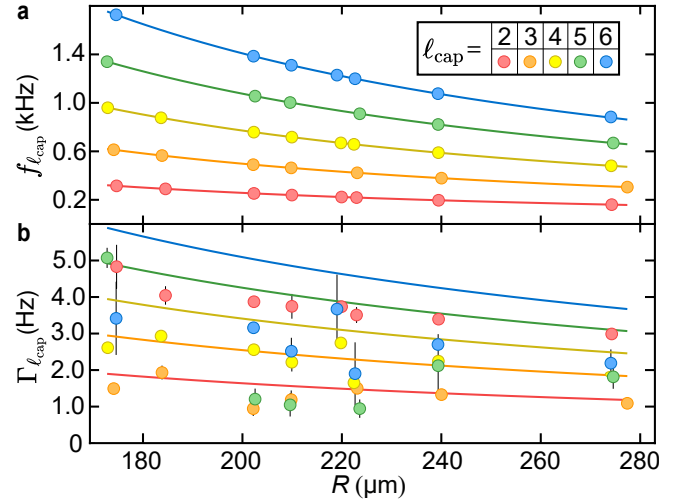

FIG. 7. The capillary modes' resonant frequencies (a) and damping rates (b) as a function of R. The circles are the data and the dotted lines are the expected values assuming $T_{\mathrm{drop}} = 350$ mK.

Fig. 7 shows the capillary modes' frequencies and linewidths as a function of the drop radius. As in Fig. 6, the frequencies show excellent agreement with Eq. 2, while the linewidths show only qualitative agreement with Eq. 3.

In conclusion, these results show that drops of superfluid ^{4}He can be magnetically levitated in high vacuum with indefinitely long lifetime, and that their thermal, optical, and mechanical properties are consistent with expectations. We expect that modest improvements in the design of the experimental cell will reduce the density of background He atoms, resulting in lower drop temperature and correspondingly lower rates of mechanical damping and evaporation. In addition, the use of *in situ* mode-matching optics should allow for access to the high-finesse $q = 1$ WGMs. The realization of such WGMs in objects whose stiffness is set by the relatively low surface tension of liquid helium may provide access to new regimes of cavity optomechanics.

[1] R. M. P. Tanyag, C. F. Jones, C. Bernando, S. M. O'Connell, D. Verma, and A. F. Vilesov, Cold chemistry: molecular scattering and reactivity near absolute zero **11**, 389 (2017).

[2] J. A. Northby, Journal of Chemical Physics **115**, 10065 (2001).

[3] F. Stienkemeier and K. K. Lehmann, Journal of Physics B-Atomic Molecular and Optical Physics **39**, R127 (2006).

[4] C. Callegari, K. K. Lehmann, R. Schmied, and G. Scoles, Journal of Chemical Physics **115**, 10090 (2001).

[5] E. Lugovoj, J. P. Toennies, and A. Vilesov, Journal of Chemical Physics **112**, 8217 (2000).

[6] J. P. Toennies and A. F. Vilesov, Annual Review of Physical Chemistry **49**, 1 (1998).

[7] S. M. O. O'Connell, R. M. P. Tanyag, D. Verma, C. Bernando, W. Pang, C. Bacellar, C. A. Saladrigas, J. Mahl, B. W. Toulson, Y. Kumagai, P. Walter, F. Ancilotto, M. Barranco, M. Pi, C. Bostedt, O. Gessner, and A. F. Vilesov, Phys. Rev. Lett. **124**, 215301 (2020).

[8] L. F. Gomez, K. R. Ferguson, J. P. Cryan, C. Bacellar, R. M. P. Tanyag, C. Jones, S. Schorb, D. Anielski, A. Belkacem, C. Bernando, R. Boll, J. Bozek, S. Carron, G. Chen, T. Delmas, L. Englert, S. W. Epp, B. Erk, L. Foucar, R. Hartmann, A. Hexemer, M. Huth, J. Kwok, S. R. Leone, J. H. S. Ma, F. R. N. C. Maia, E. Malmerberg, S. Marchesini, D. M. Neumark, B. Poon, J. Prell, D. Rolles, B. Rudek, A. Rudenko, M. Seifrid, K. R. Siefermann, F. P. Sturm, M. Swiggers, J. Ullrich, F. Weise, P. Zwart, C. Bostedt, O. Gessner, and A. F. Vilesov, Science **345**, 906 (2014).

[9] S. Chandrasekhar, Proceedings of the Royal Society of London. Series A. Mathematical and Physical Sciences **286**, 1 (1965).

[10] R. A. Brown and L. E. Scriven, Proceedings of the Royal Society of London Series a-Mathematical Physical and Engineering Sciences **371**, 331 (1980).

[11] C. J. Heine, Ima Journal of Numerical Analysis **26**, 723 (2006).

[12] L. Childress, M. P. Schmidt, A. D. Kashkanova, C. D. Brown, G. I. Harris, A. Aiello, F. Marquardt, and J. G. E. Harris, Physical Review A **96** (2017), ARTN 063842 10.1103/PhysRevA.96.063842.

[13] J. J. Niemela, Journal of Low Temperature Physics **109**, 709 (1997).

[14] M. A. Weilert, D. L. Whitaker, H. J. Maris, and G. M. Seidel, Journal of Low Temperature Physics **98**, 17 (1995).

[15] M. A. Weilert, D. L. Whitaker, H. J. Maris, and G. M. Seidel, Physical Review Letters **77**, 4840 (1996).

[16] H. Buchenau, E. L. Knuth, J. Northby, J. P. Toennies, and C. Winkler, Journal of Chemical Physics **92**, 6875 (1990).

[17] W. Schollkopf and J. P. Toennies, Science **266**, 1345 (1994).

[18] J. Braun, P. K. Day, J. P. Toennies, G. Witte, and E. Neher, Review of Scientific Instruments **68**, 3001 (1997).

[19] J. P. Toennies, A. F. Vilesov, and K. B. Whaley, Physics Today **54**, 31 (2001).

[20] J. P. Toennies and A. F. Vilesov, Angewandte Chemie-International Edition **43**, 2622 (2004).

[21] A. Kautsch, M. Koch, and W. E. Ernst, Physical Chemistry Chemical Physics **17**, 12310 (2015).

[22] P. Thaler, A. Volk, D. Knez, F. Lackner, G. Haberfehlner, J. Steurer, M. Schnedlitz, and W. E. Ernst, Journal of Chemical Physics **143** (2015), Artn 134201 10.1063/1.4932182.

[23] D. M. Brink and S. Stringari, Zeitschrift Fur Physik D-Atoms Molecules and Clusters **15**, 257 (1990).

[24] M. A. Weilert, D. L. Whitaker, H. J. Maris, and G. M. Seidel, Journal of Low Tempearture Physics **106**, 101 (1997).

[25] C. D. Brown II, *Optical, Mechanical and Thermal Properties of Superfluid Helium Drops Magnetically Levitated in Vacuum*, Ph.D. thesis, Yale University (2019).

[26] G. Seidel, R. Lanou, and W. Yao, Nuclear Instruments and Methods in Physics Research Section A: Accelerators, Spectrometers, Detectors and Associated Equipment **489**, 189 (2002).

[27] A. N. Oraevsky, Quantum Electronics **32**, 377 (2002).

[28] T. J. A. Kippenberg, *Nonlinear optics in ultra-high Q whispering-gallery optical microcavities*, Thesis (2004).

[29] C. Vicente, W. Yao, H. J. Maris, and G. M. Seidel, Phys. Rev. B **66**, 214504 (2002).

[30] P. Roche, M. Roger, and F. I. B. Williams, Physical Review B **53**, 2225 (1996).

[31] H. J. Maris, Reviews of Modern Physics **49**, 341 (1977).